This paper is among the 10 papers selected for submission of journal version to IEEE JBHI (out of 2,498 submissions to EMBC).

Robust Deformable Registration of Pre- and Post-resection Ultrasound Volumes for Visualization of Residual Tumor in Neurosurgery*

Hang Zhou[1] Hassan Rivaz[2]

***Abstract*— The brain tissue deforms significantly during neurosurgery, which has led to the use of intra-operative ultrasound in many sites to provide updated ultrasound images of tumor and critical parts of the brain. Several factors degrade the quality of post-resection ultrasound images such as hemorrhage, air bubbles in tumor cavity and the application of blood-clotting agent around the edges of the resection. As a result, registration of post- and pre-resection ultrasound is of significant clinical importance. In this paper, we propose a nonrigid symmetric registration (NSR) framework for accurate alignment of pre- and post-resection volumetric ultrasound images in near real-time. We first formulate registration as the minimization of a regularized cost function, and analytically derive its derivative to efficiently optimize the cost function. We use Efficient Second-order Minimization (ESM) method for fast and robust optimization. Furthermore, we use inverse-consistent deformation method to generate realistic deformation fields. The results show that NSR significantly improves the quality of alignment between pre- and post-resection ultrasound images.**

I. INTRODUCTION

Infiltrating nature of brain tumors makes their margins indistinct, which leads to residual tumor in as much as 64% [1] of patients. Therefore, neuro-navigation systems are commonly used in many sites where image-to-patient registration is performed by selecting corresponding landmarks in the pre-operative magnetic resonance (MR) image and on the skin. Unfortunately, this registration is inaccurate for two main reasons. First, brain tissue deforms after craniotomy and during surgery as much as 50 mm [2], which renders the pre-operative MR image inaccurate. Second, selection of corresponding landmarks on the skin and in the MR image is inaccurate, and leads to large registration errors. To allow the visualization of brain during the surgery, intra-operative MRI has been used. However, intra-operative MRI is extremely expensive and requires dedicated operation rooms and MR compatible surgical equipment.

Alternatively, intra-operative ultrasound imaging is convenient and significantly less expensive, and is therefore used in many neurological centers. An ultrasound volume is obtained before the tumor resection to allow the visualization of tumor and critical brain structures. Another ultrasound scan is acquired after the resection to help the surgeon minimize the residual tumor. Unfortunately, several factors such as hemorrhage substantially degrade the quality of post-resection ultrasound images. Therefore, registration of pre- and post-operation ultrasound volumes is of significant clinical interest. This registration is challenging for several reasons. First, brain tissue deforms during the resection, and therefore, this registration has to be deformable. Second, the intensity and contrast of the same tissue can be different in two images due to variations in the acquisition angle and location, as well as possible changes in Time Gain Compensation (TGC). And third, because of the removal of partial tissue during the resection, some regions of pre- and post-resection images do not correspond to each other.

We recently proposed an automatic registration technique called RESOUND [3], which is based on gradient descent optimization of a regularized cost function and addresses the three aforementioned challenges as follows. First, it uses free-form B-splines to model tissue deformation. Second, it uses Normalized Cross Correlation (NCC) as the similarity metric, which can be reliably computed over small patches and is also invariant to affine intensity variations. And third, it proposes a novel outlier rejection technique to find areas of non-correspondence. An important issue with RESOUND, however, is that free-form B-splines are not invertible and can generate folds and ruptures that are physically unrealistic. Another issue lies in the optimization scheme used in RESOUND, which is slow and can get trapped in local minima. This can hinder the clinical application of RESOUND where robust and accurate performance is critical.

Registration of ultrasound volumes is an active field of research with numerous new advances. Some previous work is listed below. Mercier *et al.* [4] performed deformable registration between pre- and post-resection images in neurosurgery by manually segmenting the tumor and resection cavity. Simplex optimization of a regularized cost function with cross correlation as the similarity metric is performed in the next step. Presles *et al.* [5] used intensity and gradient of ultrasound volumes in a mutual information similarity metric, and performed stochastic gradient descent optimization. Khallaghi *et al.* [6] exploited corresponding attribute vectors in the two volumes to estimate the deformable transformation. And Schneider *et al.* [7] performed feature-based rigid registration.

In this work, we build on RESOUND and propose a novel robust deformable registration technique for alignment of pre- and post-resection ultrasound images called nonrigid symmetric registration (NSR). We use symmetric deformation fields that are invertible and therefore create high quality deformation fields. In addition, we incorporate Efficient Second-order Minimization (ESM) method [8] into

[1]Hang Zhou is with Department of Electrical and Computer Engineering and PERFORM Centre, Concordia University, Montreal, Quebec, Canada z_hang@encs.concordia.ca

[2]Hassan Rivaz is with Department of Electrical and Computer Engineering and PERFORM Centre, Concordia University, Montreal, Quebec, Canada hrivaz@ece.concordia.ca

our optimization technique to allow fast and reliable convergence. We validate our technique on ultrasound images of 13 patients and show that NSR accurately registers these challenging images.

II. METHOD

A. registration

Many registration algorithms, including RESOUND, find a free-form B-spline transformation that maps one image to another. Several issues arise in such registration frameworks: the resulting transformation is not symmetric with respect to the two images, is biased towards one of the images, is not invertible, and can cause physically implausible folds or ruptures. To overcome these problems, inverse consistent registration methods have been proposed in [9], [10]. They reduce the bias by calculating forward and backward transformations $\mathbf{T_1}$ and $\mathbf{T_2}$, and penalizing the difference between $\mathbf{T_1} \circ \mathbf{T_2}^{-1}$ and the identity transformation. In this work, we use a symmetric and inverse consistent method similar to [11], and apply the iterative approach of [12] to invert transformations. The full forward and backward deformation can then be calculated as $\mathbf{T_1}(0.5) \circ \mathbf{T_2}(0.5)^{-1}$ and $\mathbf{T_2}(0.5) \circ \mathbf{T_1}(0.5)^{-1}$ respectively, where 0.5 means half of the deformation field and $\circ$ represents composition of transformations.

Let $\mathbf{V_1}$ and $\mathbf{V_2}$ represent the two ultrasound volumes, and $\mathbf{x} \subset R_d$ be the global coordinates, where $d = 3$ for 3D volumetric images. Also, $\mathbf{T_u}(\mathbf{x}) = \mathbf{x} + \mathbf{u}$ represents the forward and backward deformation. The goal of image registration is to find the 3D deformation fields $\mathbf{u_1}$ from $\mathbf{V_1}$ to $\mathbf{V_2}$ and $\mathbf{u_2}$ from $\mathbf{V_2}$ to $\mathbf{V_1}$. To find $\mathbf{u_1}$ and $\mathbf{u_2}$, a regularized cost function can be formulated as:

$$C = D(\mathbf{V_1}(\mathbf{T}_{\mathbf{u_1}(0.5)}(\mathbf{x})), \mathbf{V_2}(\mathbf{T}_{\mathbf{u_2}(0.5)}(\mathbf{x}))) + \alpha \mathrm{tr}(\nabla \mathbf{u}_1^T \nabla \mathbf{u}_1)^2 + \alpha \mathrm{tr}(\nabla \mathbf{u_2}^T \nabla \mathbf{u_2})^2 \quad (1)$$

where D is the dissimilarity metric, $\mathbf{V_1}(\mathbf{T}_{\mathbf{u_1}(0.5)}(\mathbf{x}))$ is the middle volume from $\mathbf{V_1}$, $\mathbf{V_2}(\mathbf{T}_{\mathbf{u_2}(0.5)}(\mathbf{x}))$ is the middle volume from $\mathbf{V_2}$, α is the regularization weight, tr is the trace operator and $\mathrm{tr}(\nabla \mathbf{u}^T \nabla \mathbf{u})^2$ is the diffusion regularization term.

Hierarchical registration from coarse to fine levels is also applied in this work to speed up the registration process and avoid getting trapped in local minimum.

Moreover, instead of using -NCC as the dissimilarity metric, we use $-\mathrm{NCC}^2$ to make it adapt to quadratic optimization methods. Then we divide the volume into small patches, calculating $-\mathrm{NCC}^2$ in each patch, and add the results up to generate a global cost:

$$D = -\frac{1}{N} \sum_{i=1}^{N} \rho_i^2 \quad (2)$$

$$\rho_i^2 = \frac{(\sum_{j=1}^{n} (V_{1j} - \overline{V_{1i}})(V_{2j} - \overline{V_{2i}}))^2}{\sum_{j=1}^{n} (V_{1j} - \overline{V_{1i}})^2 \sum_{j=1}^{n} (V_{2j} - \overline{V_{2i}})^2} \quad (3)$$

$$V_{1j} = \mathbf{V_1}(\mathbf{T}_{\mathbf{u_1}(0.5)}(\mathbf{x_j})), V_{2j} = \mathbf{V_2}(\mathbf{T}_{\mathbf{u_2}(0.5)}(\mathbf{x_j}))$$

where as before, D is the dissimilarity metric, $\overline{V_{1i}}$ and $\overline{V_{2i}}$ are the mean intensity of the patch i in $\mathbf{V_1}$ and $\mathbf{V_2}$ respectively, N is the number of patches in the volume and n is the number of pixels in every patch. The tumor is removed during the resection and therefore does not correspond to the resection cavity in the post-resection ultrasound image. Orientation of the descent direction of individual pixels is proposed in [13] to find outliers and limit their effect. We use this technique in this work to eliminate patches that fall in non-corresponding regions.

B. optimization

To calculate the optimal deformation fields, we have to minimize the cost function. Usually, non-linear minimization problems are solved in an iterative manner. Several optimization algorithms can be applied to obtain the incremental update. Steepest gradient descent (SGD) is used in [3] to optimize the cost function. However, SGD moves perpendicularly to the isolines and generally has a low convergence rate [8]. In this work, we use pseudo-inverse of the mean of the Jacobian matrices as the optimization method, which is one of the ESM methods [8]. ESM uses first-order derivatives to approximate second-order derivatives, making the optimization computationally efficient. In this algorithm, the forward deformation Jacobian is combined with the backward one to generate more accurate incremental updates. Despite the fact that ESM uses only first-order derivatives, it is shown to have a cubic convergence rate [14].

When we calculate the $-\mathrm{NCC}^2$ in each patch, we can also obtain the value of NCC and the derivative of NCC with respect to intensity. We assign the NCC to every pixel in that patch to act as the residual function:

$$\frac{\partial \rho_i}{\partial I} = \frac{1}{|V_1||V_2|}(V_1 - \frac{\langle V_1, V_2 \rangle}{|V_2|^2} V_2) \quad (4)$$

$$V_1 = V_{1j} - \overline{V_{1i}}, V_2 = V_{2j} - \overline{V_{2i}}$$

where ρ_i is the NCC of patch i and $\frac{\partial \rho_i}{\partial I}$ is the derivative of NCC with respect to the intensity of each pixel in patch i. Since we need the NCC value and derivative at each voxel, we define P as:

$$P = \begin{bmatrix} \rho_1 & \rho_2 & \cdots & \rho_j & \cdots & \rho_M \end{bmatrix}^T \quad (5)$$

where ρ_j is the NCC value of pixel j and M is the total number of voxels in the volume. In an abuse of notation, we define $\frac{\partial P}{\partial I}$ as:

$$\frac{\partial P}{\partial I} = \begin{bmatrix} \frac{\partial \rho_1}{\partial I_1} & \frac{\partial \rho_2}{\partial I_2} & \cdots & \frac{\partial \rho_j}{\partial I_j} & \cdots & \frac{\partial \rho_M}{\partial I_M} \end{bmatrix}^T \quad (6)$$

where $\frac{\partial \rho_j}{\partial I_j}$ is the derivative of NCC in pixel j with respect to the intensity of that pixel. Using the chain rule, we obtain:

$$\nabla_{\mathbf{u_1}} P = \frac{\partial P}{\partial \mathbf{u_1}} = \frac{\partial I_{\mathbf{V_1}}}{\partial \mathbf{u_1}} \frac{\partial P}{\partial I_{\mathbf{V_1}}} \quad (7)$$

$$\nabla_{\mathbf{u_2}} P = \frac{\partial P}{\partial \mathbf{u_2}} = \frac{\partial I_{\mathbf{V_2}}}{\partial \mathbf{u_2}} \frac{\partial P}{\partial I_{\mathbf{V_2}}} \quad (8)$$

where $\frac{\partial I_V}{\partial \mathbf{u}}$ is the gradient of intensity, $\nabla_{\mathbf{u_1}} P$ is the Jacobian of NCC with respect to the forward deformation field and $\nabla_{\mathbf{u_2}} P$ is the Jacobian with respect to the backward deformation field. Given the Jacobian of two directions, we can find the optimal deformation fields following an iterative rule. First the forward Jacobian is combined with the backward Jacobian to generate the average Jacobian, which will be used in subsequent computation:

$$\nabla_{\mathbf{u_1}} P_{new} = \frac{1}{2}(\nabla_{\mathbf{u_1}} P - \nabla_{\mathbf{u_2}} P) \tag{9}$$

$$\nabla_{\mathbf{u_2}} P_{new} = \frac{1}{2}(\nabla_{\mathbf{u_2}} P - \nabla_{\mathbf{u_1}} P) \tag{10}$$

where $\nabla_{\mathbf{u_1}} P_{new}$ and $\nabla_{\mathbf{u_2}} P_{new}$ are the average Jacobian for forward and backward deformation respectively. We use these two to replace $\nabla_{\mathbf{u_1}} P$ and $\nabla_{\mathbf{u_2}} P$ for following formulas.

Afterwards the incremental updates can be computed with the rule $(\nabla_{\mathbf{u}} P^T \nabla_{\mathbf{u}} P)\Delta_{\mathbf{u}} = \nabla_{\mathbf{u}} P^T P$, where P is the vector of NCC values. Since the regularization term is added to the cost function to solve the ill-posed problem, the update rule becomes [11]:

$$(\nabla_{\mathbf{u}} P^T \nabla_{\mathbf{u}} P + \alpha I)\Delta_{\mathbf{u}} = (\nabla_{\mathbf{u}} P^T P - \alpha \nabla^2 \mathbf{u}_{previous}) \tag{11}$$

where I is the identity matrix, α is the coefficient and $\nabla^2 \mathbf{u}_{previous}$ is the Laplacian of the summation of all previous updates. The incremental update $\Delta_{\mathbf{u}}$ is calculated using the successive over-relaxation solver. Compared with the Jacobi and Gauss-Seidel methods, it is more accurate and flexible for solving equations. Subsequently, the deformation fields can be updated by adding the incremental updates, formulas are as:

$$\mathbf{u_1}^{t+1} = \mathbf{u_1}^t + \lambda \Delta_{\mathbf{u_1}} \tag{12}$$

$$\mathbf{u_2}^{t+1} = \mathbf{u_2}^t + \lambda \Delta_{\mathbf{u_2}} \tag{13}$$

where λ is the step size, $\Delta_{\mathbf{u_1}}$ is the incremental update of forward deformation field and $\Delta_{\mathbf{u_2}}$ is the update of backward deformation field.

In each iteration, according to the definition of symmetric and inverse-consistent registration, the full deformation fields will be calculated by:

$$\mathbf{u_1}_{full} = \mathbf{u_1}(0.5) \circ \mathbf{u_2}(0.5)^{-1} \tag{14}$$

$$\mathbf{u_2}_{full} = \mathbf{u_1}(0.5)^{-1} \circ \mathbf{u_2}(0.5) \tag{15}$$

III. EXPERIMENTS AND RESULTS

To validate the performance of our registration framework, pre- and post-resection ultrasound images of 13 patients are used from the BITE database [15]. The experimental procedures involving human subjects in BITE were approved by McGill University's Institutional Review Board. These volumes are reconstructed from 2D ultrasound image sequences with the voxel size of $1 \times 1 \times 1$ mm^3. This database also includes corresponding homologous anatomical landmarks in pre- and post-resection ultrasound volumes. To quantitatively measure the performance of NSR, we use the mean target registration errors (mTRE) metric, which is the distance between these landmarks. To calculate mTRE, let $\mathbf{x}$ and $\mathbf{x}'$ represent the corresponding landmarks in $\mathbf{V_1}$ and $\mathbf{V_2}$ respectively. Therefore mTRE can be calculated as [16]:

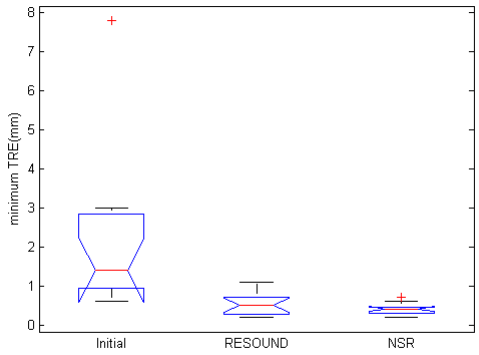

Fig. 1. The boxplot of minimum TRE.

$$\text{mTRE} = \frac{1}{n}\sum_{i}^{n} \|\mathbf{T_{u_1}}(\mathbf{x_i}) - \mathbf{x_i'}\| \tag{16}$$

where $\mathbf{T_{u_1}}$ is the forward deformation and n is the number of landmarks.

The original mTRE and final mTRE of all patients are shown in Table I. NSR takes approximately 20 seconds on a 3GHz processor to perform a typical 3D registration. As can be seen from the table, every mTRE decreases to a relatively small value after registration. Even the mTRE of the patient 11, whose initial value of 10.5 mm is decreased to 2.8 mm after registration. Also, the distribution of minimum TRE is shown in Fig. 1. Compared with RESOUND, NSR provides similar mTRE and better minimum TRE using fewer iterations. This improvement is caused by both improved optimization and inverse consistent registration of NSR.

In order to visually demonstrate the effect of our registration framework, pre- and post-registration alignment of images of two patients are shown in Fig. 2. Here, we choose one frame from the pre-resection volume and automatically find edges using a Canny edge detector. Fig. 2 (a) shows the Canny edge of the frame from the pre-resection volume, and Fig. 2 (b) shows the initial alignment of the contour and the post-resection frame before registration. We can find that the contour and the frame do not correspond well. Fig. 2 (c) shows the alignment after NSR, and it provides a distinct evidence for judging the residual tumor. Fig. 2 (d) shows the result of RESOUND. As can be seen from the comparison between (c) and (d), the final alignment of NSR is significantly better than the RESOUND's result. Arrows point to differences between alignment of RESOUND and NSR. Such qualitative results have significant advantages over mTRE because they show the level of alignment over a much larger region, compared to few points used in mTRE

TABLE I

MTRE VALUES BEFORE AND AFTER REGISTRATION WITH RESOUND AND NSR. LGG AND HGG REPRESENT LOW AND HIGH GRADE GLIOMA RESPECTIVELY. RESOUND DATA ARE FROM [3] AND ALL SMALLER VALUES ARE IN BOLD.

Patient	Tumor type	Tumor size(cm^3)	Initial	RESOUND	NSR
P1	LGG	79.2	2.3(0.6-5.4)	1.8(0.5-4.0)	**1.4**(0.3-3.9)
P2	HGG	53.7	3.9(2.8-5.1)	1.4(0.5-1.9)	**1.2**(0.6-2.4)
P3	HGG	31.6	4.6(3.0-5.9)	1.4(0.7-2.2)	**1.1**(0.3-2.2)
P4	HGG	0.2	4.1(2.6-5.5)	1.2(0.3-2.4)	**1.1**(0.2-2.0)
P5	HGG	32.3	2.3(1.4-3.1)	**1.0**(0.2-1.7)	1.2(0.7-2.4)
P6	HGG	13.9	4.4(3.0-5.4)	**1.0**(0.4-1.7)	1.0(0.6-1.7)
P7	HGG	63.1	2.7(1.7-4.1)	1.7(0.9-3.6)	**1.6**(0.2-3.7)
P8	HGG	4.8	2.2(1.0-4.6)	1.4(0.6-3.2)	**1.3**(0.4-3.4)
P9	HGG	10.4	3.9(1.0-6.7)	**1.9**(0.7-4.1)	2.6(0.4-4.9)
P10	LGG	39.7	2.9(0.8-9.0)	2.2(0.6-5.3)	**2.1**(0.4-5.9)
P11	LGG	49.1	10.5(7.8-13.0)	**2.5**(1.1-4.2)	2.8(0.3-6.4)
P12	HGG	31.9	1.6(1.3-2.2)	**0.7**(0.2-1.6)	0.8(0.4-1.4)
P13	LGG	37.3	2.2(0.6-4.0)	**1.3**(0.2-2.8)	1.3(0.4-3.0)
mean	-	34.4	3.7(2.1-5.7)	**1.5**(0.5-3.0)	**1.5**(0.4-3.3)

(around 9/patient in this dataset).

IV. CONCLUSIONS

A novel robust technique is proposed in this work for deformable registration of pre- and post-resection volumetric ultrasound images of neurosurgery. NCC, which is invariant to affine distortions of intensity values, is used as the similarity metric. ESM method is used to optimize the regularized cost function to achieve fast and reliable registration. We also use inverse-consistent deformation method to generate more realistic deformation fields. NSR outperforms RESOUND, as indicated in Fig. 2, for two main reasons: improved deformation model and more reliable optimization scheme.

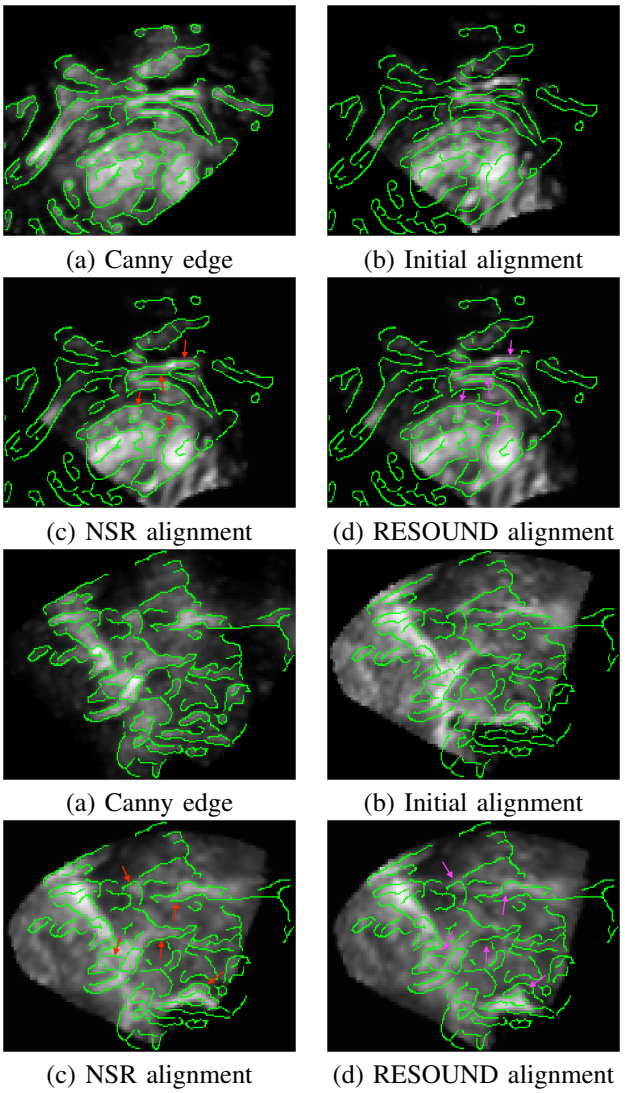

Fig. 2. The improvement of alignment after NSR and the comparison between NSR and RESOUND. All more accurately aligned regions of NSR are pointed by red arrows in (c) and magenta arrows in (d) correspondingly.

REFERENCES

[1] W. Stummer, U. Pichlmeier, T. Meinel, O. D. Wiestler, F. Zanella, and H. J. Reulen, "Fluorescence-guided surgery with 5-aminolevulinic acid for resection of malignant glioma: a randomised controlled multicentre phase III trial." Tech. Rep. 5, 2006.

[2] A. Nabavi, P. M. Black, D. T. Gering, C. F. Westin, V. Mehta, R. S. Pergolizzi, M. Ferrant, S. K. Warfield, N. Hata, R. B. Schwartz, W. M. Wells III, R. Kikinis, and F. A. Jolesz, "Serial Intraoperative MR Imaging of Brain Shift," *Neurosurgery*, vol. 48, pp. 787–798, 2001.

[3] H. Rivaz and D. L. Collins, "Near Real-Time Robust Non-rigid Registration of Volumetric Ultrasound Images for Neurosurgery," *Ultrasound Med. Biol.*, vol. 41, no. 2, pp. 574–587, 2015.

[4] L. Mercier, D. Araujo, C. Haegelen, R. F. Del Maestro, K. Petrecca, and D. L. Collins, "Registering Pre- and Postresection 3-Dimensional Ultrasound for Improved Visualization of Residual Brain Tumor," *Ultrasound Med. Biol.*, vol. 39, no. 1, pp. 16–29, 2013.

[5] B. Presles, M. Fargier-Voiron, M. C. Biston, R. Lynch, A. Munoz, H. Liebgott, P. Pommier, S. Rit, and D. Sarrut, "Semi-automatic registration of 3d transabdominal ultrasound images for patient repositioning during postprostatectomy radiotherapy," *Med. Phys.*, vol. 41, no. 12, p. 122903, 2014.

[6] S. Khallaghi, C. G. Leung, K. Hastrudi-Zaad, P. Foroughi, C. Nguan, and P. Abolmaesumi, "Experimental validation of an intrasubject elastic registration algorithm for dynamic-3d ultrasound images," *Med. Phys.*, vol. 39, no. 9, pp. 5488–5497, 2012.

[7] R. J. Schneider, D. P. Perrin, N. V. Vasilyev, G. R. Marx, J. Pedro, and R. D. Howe, "Real-time image-based rigid registration of three-dimensional ultrasound," *Med. Image Anal.*, vol. 16, no. 2, pp. 402–414, 2012.

[8] E. Malis, "Improving vision-based control using efficient second-order minimization techniques," *IEEE Int. Conf. Robot. Autom. 2004. Proceedings. ICRA '04. 2004*, vol. 2, pp. 1843–1848, 2004.

[9] G. E. Christensen and H. J. Johnson, "Consistent image registration," *IEEE Trans. Med. Imag.*, vol. 20, no. 7, pp. 568–582, 2001.

[10] D. Shen and C. Davatzikos, "HAMMER: hierarchical attribute matching mechanism for elastic registration," *IEEE Trans. Med. Imag.*, vol. 21, no. 11, pp. 1421–1439, November 2002.

[11] M. P. Heinrich, M. Jenkinson, M. Bhushan, T. Matin, F. V. Gleeson, S. M. Brady, and J. A. Schnabel, "MIND: Modality independent neighbourhood descriptor for multi-modal deformable registration," *Med. Image Anal.*, vol. 16, no. 7, pp. 1423–1435, 2012.

[12] M. Chen, W. Lu, Q. Chen, K. J. Ruchala, and G. H. Olivera, "A simple fixed-point approach to invert a deformation field," *Med. Phys.*, vol. 35, no. 1, pp. 81–88, 2008.

[13] H. Rivaz, S. J. S. Chen, and D. L. Collins, "Automatic Deformable MR-Ultrasound Registration for Image-Guided Neurosurgery," vol. 34, no. 2, pp. 366–380, 2015.

[14] E. Malis, "Vision-based estimation and robot control," Ph.D. dissertation, University Nice Sophia Antipolis, 2008.

[15] L. Mercier, R. F. Del Maestro, K. Petrecca, D. Araujo, C. Haegelen, and D. L. Collins, "Online database of clinical MR and ultrasound images of brain tumors." *Med. Phys.*, vol. 39, no. 6, pp. 3253–3261, Jun. 2012.

[16] P. Jannin, J. M. Fitzpatrick, D. J. Hawkes, X. Pennec, R. Shahidi, and M. W. V. Annier, "Validation of medical image processing in image-guided therapy," *Neurosurgery*, vol. 21, no. 2, pp. 1445–1449, 2002.